Radar–Acoustic Detection of Aircraft Wake Vortices

WILLIAM L. RUBIN

WLR Research Inc., Whitestone, New York

(Manuscript received 21 June 1999, in final form 13 October 1999)

ABSTRACT

All aircraft produce trailing wake vortices as a direct consequence of generating lift. Vortices may be dangerous to following aircraft during takeoff and landing. An all-weather airport wake vortex sensor has been sought for more than 25 years as part of a ground-based wake vortex avoidance system that would enable current U.S. Federal Aviation Administration separation standards to be safely reduced under instrument and visual flight rule conditions. A sensitive all-weather radar–acoustic wake vortex sensor is described that satisfies wake vortex avoidance system requirements. Samples of recent vortex data gathered at New York's Kennedy International Airport are presented.

1. Introduction

The phenomenon of *lift* transforms an aircraft's engine power into a pair of counterrotating *horizontal tornados,* each about 30 to 50 m in diameter, which can stretch for kilometers behind each aircraft wingtip. Known as wingtip or wake vortices, they are visible at high altitude as contrails but are invisible near the ground. Research on wake vortices dates back at least to the 1930s (Betz 1932).

Wake vortices may be dangerous to following aircraft during landing and takeoff (Hallock 1991). Following the introduction of jumbo jet aircraft in the 1970s, the U.S. Federal Aviation Administration (FAA) increased mandated minimum spacings from a uniform 3 nmi (5.5 km) separation between leader and follower aircraft to between 3 and 6 nmi (5.5 and 11 km), depending on the weight classfication of the lead and following aircraft (Hallock 1991).

Following the increase in separation standards, two major approaches have been pursued to reduce their negative impact on air traffic flow. One has been to alter the vortex generating characteristics of aircraft through design changes. This approach has met with limited success. In the second approach, so-called wake vortex avoidance systems have been investigated whose aim is to replace fixed separation standards by adaptive separation standards. Extensive vortex field data indicates separations as low as 2 nmi (3.7 km) can be safely used 90% of the time (Hallock 1991). Wake vortex avoidance systems typically (a) use meteorological forecast methods to predict vortex movements and decay in airport air corridors, (b) confirm and update predicted vortex behavior based on observations from an onsite vortex sensor, (c) forecast safe aircraft separations, and (d) provide a waveoff capability when a vortex unpredictably strays into an air corridor.

To accomplish their objective, wake vortex avoidance systems require a wake vortex sensor with the following characteristics: (i) adequate vortex detection/measurement sensitivity under all weather conditions, (ii) real-time operation, (iii) computerized interface, and (iv) compatibility with airport operational constraints. Many candidate technologies have been investigated over the last 25 years (Hallock and Aberle 1977; Hallock 1991; Burnham 1997). They include microwave and millimeter wave radar, sodar, lidar, and anemometer-based ground wind lines. Each falls short in varying degrees with respect to the above criteria.

A radar–acoustic wake vortex sensor described in this paper was tested at New York's John F. Kennedy International Airport (JFK) over the period 1994–98. These tests showed that the sensor not only satisfied all of the above criteria but also detected vortices generated by small aircraft, a capability lacking in most other sensors. [Small aircraft weigh $<$41 000 lb ($<$18 600 kg), large between 41 000 (18 600 kg) and 255 000 lb (115 700 kg), and a heavy aircraft is $>$255 000 lb ($>$115 700 kg).]

Radar–acoustic sensing is a well-established technique for measuring vertical temperature profiles of the atmosphere. The hardware and software of a standard National Oceanic and Atmospheric Administration (NOAA) radar–acoustic sensor which makes measurements all over the world was modified for vortex de-

Corresponding author address: Dr. William L. Rubin, WLR Research Inc., 166-47 16 Avenue, Whitestone, NY 11357.
E-mail: wrubin@i-2000.com

tection. Sensor electronics were housed in a small unheated trailer box at JFK and suffered only a few contact problems during 6 yr of operation.

For completeness, it should be mentioned that the acoustic emission of radar–acoustic sensors used for atmospheric measurements have been found to be annoying. This criticism is less valid for an airport wake vortex sensor for two reasons. First, the sensor is acoustically silent until an aircraft is detected in its radar beam, and acoustic emission ceases after 180 s, unless a following aircraft has in the meantime passed through the sensor's radar beam (180 s has been found to be a practical upper limit for which vortices remain hazardous in an air corridor). Second, sensor operation would most likely be limited to periods of high airport traffic, during which time aircraft noise is generally louder than the sensor's acoustic emission.

2. Background: Radar–acoustic sensing

Conventional radar backscatter from clear air is due to minute natural fluctuations in the air's index of refraction. Vertical wind profilers, which depend on clear-air radar backscatter, typically integrate returns for several minutes in order to extract atmospheric wind data. However, integration times longer than several seconds are not compatible with wake vortex measurements.

A radar–acoustic sensor radiates overlapping radar and acoustic beams, the latter enhancing radar backscatter by more than 40 dB relative to clear-air return. This technique was first employed at Stanford University in the 1970s to measure the vertical temperature profile of the lower atmosphere (Marshall 1970; Marshall et al. 1972; North et al. 1973). This technique is currently in wide use in the meteorological community. Recent U.S. activity has focused on incorporating radar–acoustic temperature sensing into existing wind profiler radars (Currier et al. 1988; May et al. 1989; Strauch et al. 1989).

Because the air's index of refraction is a function of density, an acoustic wave, which consists of a spatial sequence of condensations and rarefactions, produces analogous in situ variations in the air's refraction index. Radar pulses reflect from the acoustically induced index variations, the reflected signal being largest when the acoustic wavelength is one-half the radar wavelength (Bragg effect). In this case, electric fields reflecting from each acoustic condensation and rarefaction add in phase at the radar receiving antenna.

Because the radar and acoustic radiators are collocated and point in the same direction, both radar and acoustic wavefronts have identical overlapping spherical shapes. Under these conditions, radar reflections at all ranges focus onto the radar antenna (Clifford et al. 1978). Signal-to-noise (SNR) improvements produced by focused reflection and Bragg enhancement enable a 10-W (average) pulse Doppler radar and a 100-W (average) acoustic radiator to generate output SNRs greater than 20 dB out to 1 km and beyond. Since SNR is a function of both radar and acoustic signal power levels, one can be traded off against the other with no effect on performance. However, it is generally more cost effective to utilize higher acoustic than RF power.

It is relatively straightforward to show that the Bragg acoustic frequency is equal to the radar Doppler frequency corresponding to the speed of sound. The vortex sensor's radar operates at 915 MHz, in which case the Bragg acoustic frequency (and therefore the Doppler frequency corresponding to the speed of sound) is approximately 2 kHz for normal atmospheric temperatures.

As is well known, crosswinds have an adverse effect on the SNR of radar–acoustic sensors. A crosswind shifts the sensor's acoustic beam in a transverse direction (out of the radar beam) by an amount that increases with range and crosswind speed. The method used to reduce this loss is to add an acoustic radiator on each side of the principal acoustic radiator. Depending on crosswind direction, at farther ranges an auxiliary acoustic beam enters the radar beam as the principal acoustic beam moves out.

3. Vortex sensing

When a (radiated) acoustic wave traveling at the speed of sound passes transversely through the rotational flow of a vortex, segments of the acoustic wavefront in the upper (lower) half of the vortex speed up, while other segments in the lower (upper) half slow down, in both cases by amounts that depend on distance from the vortex center. (The rotational flow also causes slight vertical shifts and some distortion of the acoustic beam as it passes through a vortex, both resulting in a small SNR reduction.) It is shown in appendix A that the received radar Doppler spectrum is uniquely related to the vortex's spatial velocity distribution. In appendix B it is shown that the second moment of the measured vortex Doppler spectrum, raised to the 2/3 power, is proportional to vortex circulation (strength).

The fact that the measured vortex Doppler spectrum is centered around the speed of sound is advantageous from a measurement point of view. It results in wide separation between the vortex Doppler spectrum and competing Doppler spectra of ground clutter and aircraft echoes, also received by the sensor, since wind and aircraft speeds near an airport are much smaller than the speed of sound.

A major advantage of a radar–acoustic sensor in a vortex avoidance system is that the sensor's SNR increases in poor visibility (rain and fog) since high humidity significantly reduces acoustic attenuation. The reverse is true, for example, for laser sensors. This is operationally important since the responsibility for safe separation lies with pilots under visual flight rules (VFRs), and with controllers under instrument flight rules (IFRs). In VFR operations, pilots tend to use closer

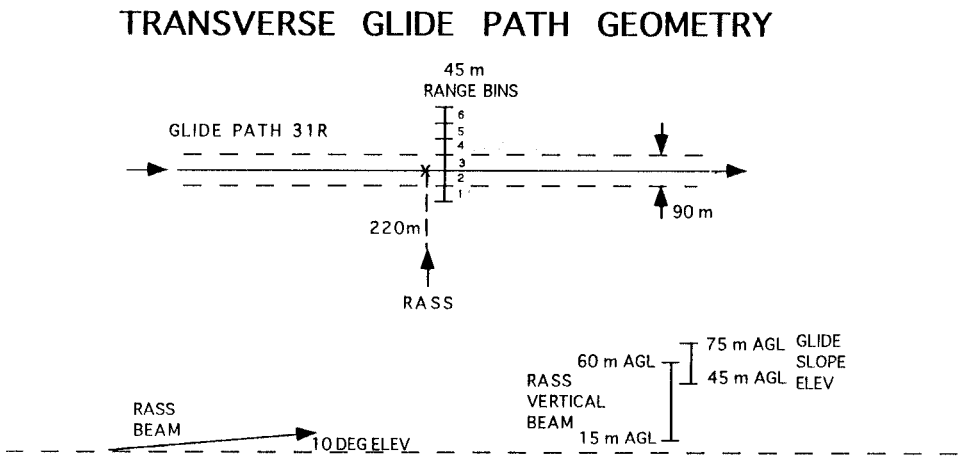

FIG. 1. The diagrams depict radar–acoustic sensing geometry used in Oct 1998 tests at JFK to detect wake vortices in glide path 31R.

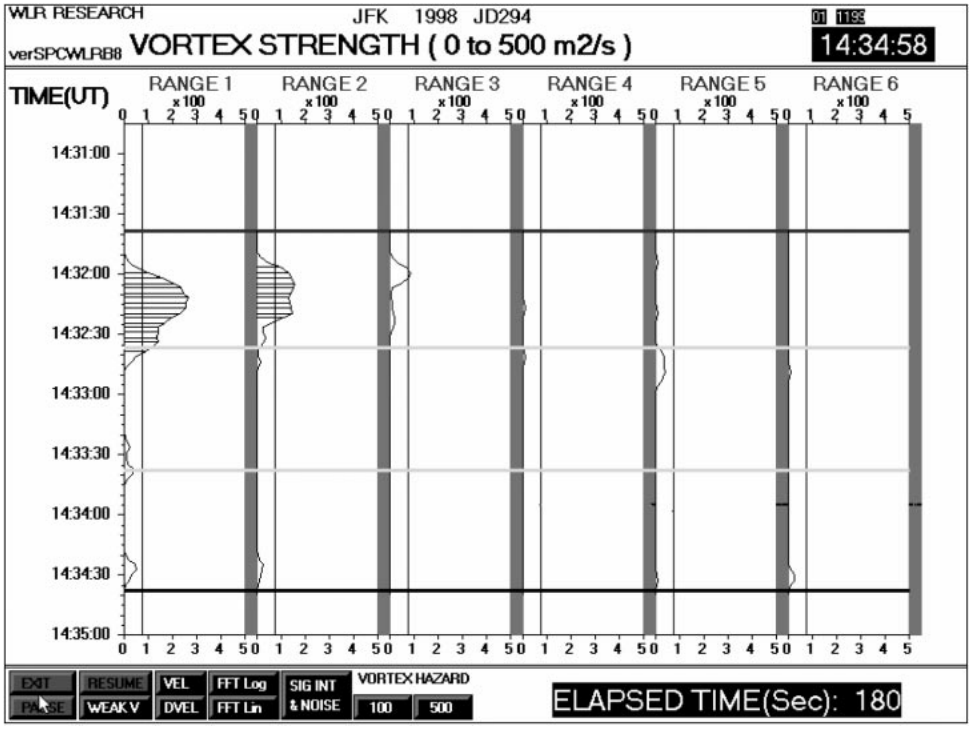

FIG. 2. This is what the screen of the sensor's real-time display looked like at 1434:58 UTC on Julian day 294 (21 Oct 1998). It shows vortices generated by an MD83 aircraft landing at JFK. The aircraft passed through the sensor's radar beam at 1431:38 UTC at which time the sensor's acoustic beam was automatically energized. The vortex closer to the sensor apparently escaped detection due to a strong crosswind component toward the sensor. The farther vortex is first observed descending into range bin 3 and moving rapidly into range bin 2 and then range bin 1. (Horizontal lines to the left of data points are drawn only when vortex circulation exceeds 75 $m^2\ s^{-1}$.) By 1432:30 UTC the vortex had pretty much moved closer and out of range bin 1. Maximum circulation of approximately 275 $m^2\ s^{-1}$ was recorded in range bin 1. The horizontal bands overlaying the display are separated by 60 s, beginning with aircraft arrival. Acoustic emission, and thus vortex detection, stopped automatically 180 s after the aircraft passed through the sensor's beam. Elapsed time since aircraft arrival is shown at the screen bottom. Current time is shown on the upper right.

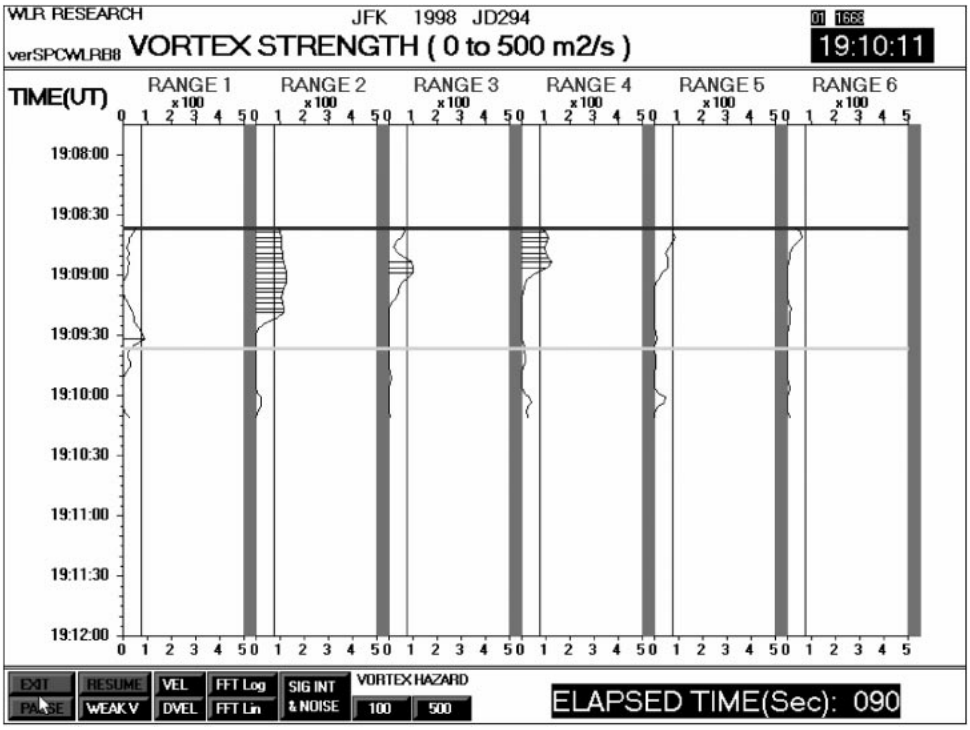

FIG. 3. This screen recorded at 1910:11 UTC shows vortices generated by a Saab 340B that passed through the sensor's radar beam at 1908:36 UTC. One vortex appears to be in range bin 2 and the second in range bin 4 with some overlapping detections in adjacent range bins. Both vortices appear to be moving slowly toward the sensor before decaying. Probably beause the Saab 340B is a small aircraft whose vortices are not considered dangerous, a following aircraft arriving 90 s later aborted the Saab 340B screen display (see elapsed time meter at bottom), at which time a new screen was automatically initiated for the following aircraft.

spacings than those mandated for IFR because they can employ vortex avoidance procedures such as flying above the flight path of a preceding aircraft. As a result, airport traffic delays are greater during IFR conditions (poor weather).

4. 1998 test setup

In the October 1998 tests at JFK, the vortex sensor was positioned to one side of glide path 31R near the middle marker, about 220 m from the extended runway centerline (see Fig. 1). The sensor's overlapping radar and acoustic beams each had a vertical beamwidth of 12° and both were pointed perpendicular to the glide path at an elevation angle of 10°. The vertical height of the glide slope near the middle marker stretches from 45 to 75 m AGL, while the vortex sensor's vertical coverage at the glide path extended from 15 to 60 m AGL. This beam coverage was chosen since vortices typically sink toward the ground after they are generated. However, the geometry results in a delay of several seconds before newly generated vortices fully enter the vortex sensor's beams. Further, a vortex must descend well into the sensor beam to accurately measure peak vortex strength. A dual-beam sensor would not have these limitations.

Vortex data was collected in each of six 45-m range bins. The boundary between range bins 2 and 3 were centered on the extended runway centerline. The Vortex Advisory System proposed by the Volpe National Transportation Systems Center (Spitzer et al. 1977), as well as the Aircraft Vortex Spacing System (Hinton 1996) proposed by the National Aeronautics and Space Administration (NASA), each define a safety corridor of ± 45 m with respect to the runway's centerline. Thus range bins 2 and 3 together monitor the safety corridor for vortex presence. Sensor signal processing converted received vortex spectra into measurements of vortex circulation (strength). For test purposes, the sensor's output was recorded and also displayed on a remote computer screen in real time.

5. Sample data

Sample real-time screen data taken during the test are shown in Figs. 2–5. In these figures, vortex circulation in each of six range bins are displayed horizontally in a waterfall-type format. For test purposes, vortex cir-

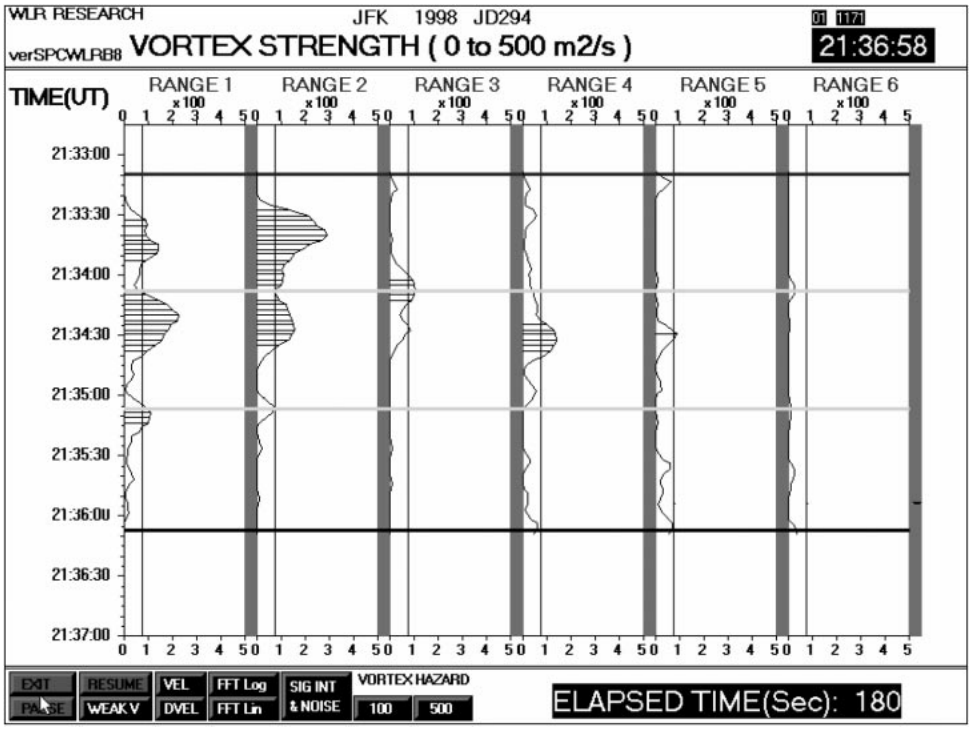

FIG. 4. The closer vortex of a B757 appears to have remained in range bins 1 and 2 until it decayed. The farther vortex, which was either weak, or only partially descended into the sensor beam in range bin 3, moved from range bin 3 to 4 where it decayed. Maximum recorded vortex circulation was approximately 300 m^2 s^{-1} in range bin 2. Vortex detection ceased after 180 s at which time the sensor's acoustic emission automatically stopped.

culation calibration was achieved by comparing measurements (Rubin et al. 1999) for different aircraft types and selecting a gain constant that provided a reasonably good fit to the collected data.

When a vortex circulation data point exceeds 75 m^2 s^{-1}, the software draws a horizontal line to the left of the data point. This helps to visually distinguish vortices from transients caused by wind gusts and passing aircraft turbulence. (The software also contains an adjustable sensitivity threshold that eliminates most nonvortex related turbulence.)

The display screen fills from top to bottom in real time with univeral time coordinated (UTC) labels on the left. Each successive aircraft arrival triggers a new screen. An overlaying horizontal band indicates aircraft arrival time. Two intermediate horizontal bands, 60 s apart, and a final horizontal band that appears at the end of 180 s, facilitate visual estimation of vortex duration in any range bin. In addition, a clock at the screen bottom shows elapsed time since an aircraft passed through the sensor's radar beam.

Discussion of the figures requires some cautionary remarks. First, the tested vortex sensor was designed to detect vortices in and around the glide path and provide a rough estimate of vortex strength, not analyze vortex behavior. The latter would probably require at least two elevation beams and increased range resolution. (Range resolution is limited by U.S. Federal Communications Commission bandwidth regulations.) Second, vortex behavior, which is described in detail in Hallock (1991), is a stochastic process in which atmospheric effects play a major role.

Prior data (Hallock 1991) show that vortices move horizontally with the ambient wind unless they are near the ground. Under calm conditions, the two counterrotating vortices tend to move in opposite directions in ground effect at a rate of 1–2 m s^{-1}. Under the influence of a crosswind over 4 m s^{-1}, both vortices move in the same direction as the crosswind, the downwind vortex moving slightly faster and the upwind slightly slower. For crosswinds around 2–3 m s^{-1}, the upwind vortex tends to move either slowly away or stall near the runway centerline, creating a potentially hazardous situation. In addition, vortex pairs often tilt or bank, possibly due to assymmetries during vortex generation or crosswind shear effects.

Keeping the above in mind, the following is offered as possible explanations of vortex behavior in Figs. 2–5. On Julian day 294 wind speed was about 3–5 m s^{-1} up glide slope 31R with a crosswind component that shifted from side to side during the day. Figure 2 shows the vortices generated by an MD83 aircraft. The farther

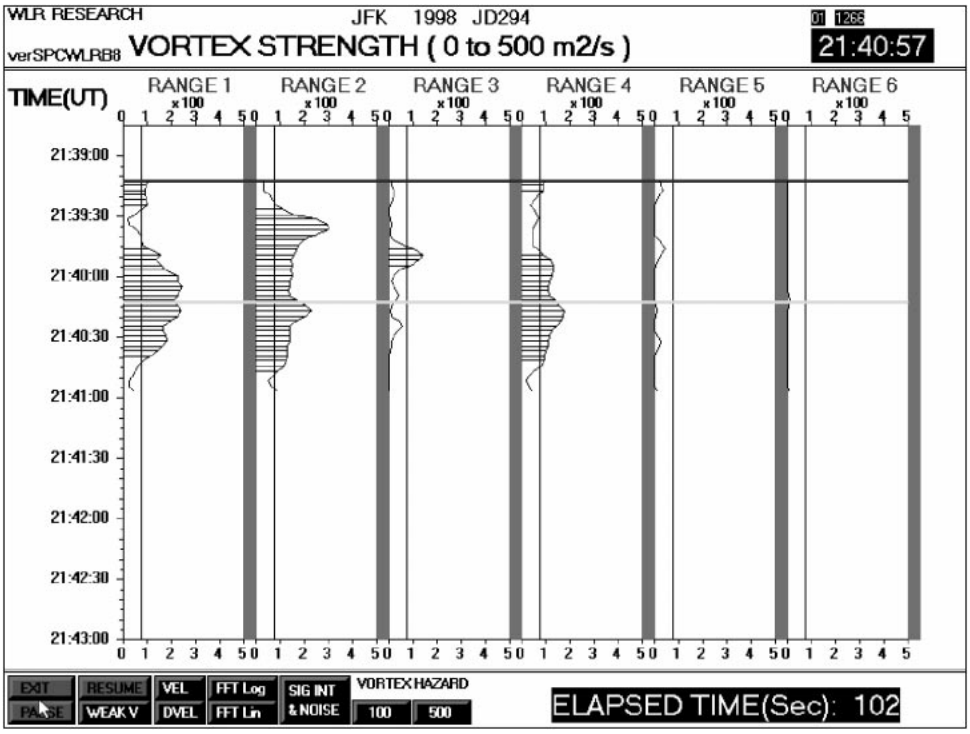

FIG. 5. Vortices are shown for an A300 aircraft that landed about 6 min after the B757 whose vortices are shown in Fig. 4. Vortex behavior appears similar to that in Fig. 4, presumably due to similar atmospheric conditions. Again maximum circulation appears in range bin 2, about 310 $m^2\ s^{-1}$. The A300 screen was interrupted by a following aircraft 102 s after its arrival, at which time its vortices were decaying, similar again to the behavior of B757 vortices in Fig. 4.

vortex appears to be only partially in the sensor beam in range bin 3 and moving toward bins 2 and 1 (closer to the radar). The closer vortex apparently escaped detection by moving rapidly toward the radar before it descended into the sensor beam.

Figure 3 shows the vortices of a Saab 340B, one in range bin 2 and one in bin 4 with some bin overlapping. Both decayed in less than 60 s. The elapsed time meter at the screen bottom indicates screen data was interrupted 90 s after the Saab entered the sensor beam by the arrival of a following aircraft, which automatically initiated a new screen.

Figure 4 is more difficult to interpret. The closer vortex of a B757 appeared to remain in range bins 1 and 2 until it decayed. The farther vortex was either weak, or only partially descended into the sensor beam, as it moved from bin 3 to 4 where it decayed. Similar behavior is observed in Fig. 5 for the vortices of an A300, which landed about 6 min later. As the elapsed time meter shows, a following aircraft arriving 102 s later interrupted the A300 screen data, at which time its vortices appear to be decaying, again similar to the behavior of B757 vortices.

6. Summary

An experimental radio-acoustic sounding system wake vortex sensor has demonstrated all-weather performance that meets the vortex sensing requirements of an automated wake vortex avoidance system. The sensor's present single beam and 45-m range bins limit the accuracy of vortex circulation measurements. A vertically scanning laser could be used to calibrate the radar–acoustic sensor's measurement of vortex circulation in clear weatherr. (Laser performance is inadequate under IFR conditions.) Present plans are to build an upgraded sensor with experimental electronics replaced by assemblies fabricated to commercial standards.

Acknowledgments. The author received an FAA research contract to demonstrate a proprietary (Rubin 1993) radar–acoustic wake vortex sensor (1992–94). Tests at JFK (1994–98) were supported by the FAA, NASA, and Volpe Center. Bob Rudis (Volpe Center) and Dr. Dave Burnham rendered much appreciated assistance during sensor testing. The author is grateful to Jim Jordan and Dr. Dave Carter (NOAA) for equipment support and many helpful discussions, and to Dr. Robert Danehy for his contributions to the vortex signal processing software. The author also acknowledges the Port Authority of New York and New Jersey, who furnished test sites at Kennedy and LaGuardia Airports (1992–98), and the JFK tower for changing the runway in use, when safe.

APPENDIX A

Relation between Vortex Flow and Vortex Spectrum

A viscous vortex consists of a swirling flow field with approximately circular streamlines. In the Rankine vortex model (Hallock and Aberle 1977), tangential velocity V_r along flow streamlines increases linearly with radius r within a small core of radius r_c, and decreases inversely with radius r outside the core. Maximum velocity $V_{\max}$, which may approach 50% of flight speed, occurs at the outside core edge. This can be stated mathematically:

$$\text{inside core:} \qquad V_r = (r/r_c)V_{\max} \qquad 0 \le |r| \le r_c \quad \text{(A1)}$$

$$\text{outside core:} \qquad V_r = (r_c/r)V_{\max} \qquad r_c \le |r|. \quad \text{(A2)}$$

As an acoustic wave propagates through a vortex, the propagation velocity of different segments of the acoustic wavefront is altered by the vortex streamlines. Streamlines in the upper half and lower half of a vortex, respectively, generate opposite sides of the vortex spectrum. For simplicity, the small spectral contribution of the core is ignored. Also, with no loss in generality, the spectrum generated by a vortex is derived assuming the speed of sound to be zero.

Let $S(V_i)$ denote the spectral magnitude of a Doppler velocity bin of width ΔV associated with velocity V_i. Using a cylindrical coordinate system with origin at the vortex center and assuming uniform scattering probability, $S(V_i)$ is given by

$$S(V_i) = \int_{-\pi/2}^{\pi/2} \int_{r(V_i)}^{r(V_i+\Delta V)} V_i \, d\theta \, r \, dr \quad \text{(A3a)}$$

$$S(V_i) = \int_{-\pi/2}^{\pi/2} \int_{r(V_i)}^{r(V_i+\Delta V)} V_r \cos\theta \, d\theta \, r \, dr. \quad \text{(A3b)}$$

Vortex circulation $\Gamma(r)$ at radius r outside the core, is given by (Hallock and Aberle 1977)

$$\Gamma(r) = \int_0^{2\pi} r \, V_r \, d\theta = \int_0^{2\pi} r(r_c/r)V_{\max} \, d\theta = 2\pi r_c V_{\max} = \Gamma, \quad \text{(A4)}$$

which is independent of radius. Equation (A2) may therefore be rewritten as

$$V_r = (r_c/r)V_{\max} = \frac{\Gamma}{2\pi r} \qquad r_c \le |r|. \quad \text{(A5)}$$

Substituting (A5) into (A3b) yields

$$S(V_i) = (\Gamma/\pi) \int_{-\pi/2}^{\pi/2} \int_{r(V_i)}^{r(V_i+\Delta V)} \cos\theta \, d\theta \, dr = \int_{-\pi/2}^{\pi/2} \int_0^{\cos\theta \, \Gamma/(2\pi V_i)} r \, dr. \quad \text{(A6)}$$

The θ integration in Eq. (A6) cannot be performed simply because V_i is a function of both r and θ. An approximate result can be obtained by assuming a core with zero radius, finding area A inside the curve defined by fixed $V_i = V_r \cos\theta = (\Gamma \cos\theta)/[2\pi \, r(V_i)]$, and taking the differential of A as V_i is varied. Thus,

$$A = \text{area for } V > V_i = \int_{-\pi/2}^{\pi/2} d\theta \int_0^{r(V_i)} r \, dr = \int_{-\pi/2}^{\pi/2} d\theta \int_0^{\cos\theta \, \Gamma/(2\pi V_i)} r \, dr \quad \text{(A7)}$$

$$A = \int_{-\pi/2}^{\pi/2} d\theta [r^2/2]_0^{\cos\theta \, \Gamma/(2\pi V_i)} = (1/2)(\Gamma/2\pi V_i)^2 \int_{-\pi/2}^{\pi/2} \cos^2\theta \, d\theta$$

$$A = \frac{\Gamma^2}{16\pi V_i^2} \quad \text{(A8)}$$

$$S(V_i) = \frac{dA}{dV_i} = \frac{\Gamma^2}{8\pi V_i^3}. \quad \text{(A9)}$$

APPENDIX B

Relation between Vortex Spectrum and Vortex Circulation

The second moment about zero is calculated for $S(V_i)$ raised to the 2/3 power:

$$\text{2nd moment} = 2 \int_{V_{\min}}^{V_{\max}} V_i^2 [S(V_i]^{2/3} \, dV_i \Big/ \int_{V_{\min}}^{V_{\max}} [S(V_i]^{2/3} \, dV_i = k_1 \int_{V_{\min}}^{V_{\max}} dV_i \Big/ \int_{V_{\min}}^{V_{\max}} (1/V_i^2) \, dV_i,$$

where $S(V_i)$ is given by Eq. (A9) and $V_{\min}$ defines the outer boundary of the vortex ($V_{\min}$ is chosen to exclude atmospheric turbulence). Performing the indicated operations,

$$\text{2nd moment} = k_1 V_{\max} V_{\min} = k_2 V_{\max}.$$

Equation (A4) in appendix A shows that vortex circulation Γ outside the core is proportional to $V_{\max}$. Hence,

$$\Gamma = k_3 \, \{\text{2nd moment of } [S(V_i)]^{2/3}\}.$$

In practice, not much difference in sensor performance was observed when the second moment was evaluated for $S(Vi)$ to the first power and the gain constant readjusted for a good fit to measured circulation.

REFERENCES

Betz, A., 1932: Behavior of vortex systems. *Z. Angew. Math. Mech.*, **12,** 164–174.

Burnham, D. C., 1997: November 1996 Kennedy Airport wake vortex test: Sensor evaluation. U.S. Dept. of Transportation Project Memo. DOT-VNTSC-FA727-PM-27.

Clifford, S. F., T. Wang, and J. T. Priestly, 1978: Spot size of the radar return from a radar–acoustic sounding system due to atmospheric refractive turbulence. *Radio Sci.,* **13,** 985–989.

Currier, P. E., W. L. Ecklund, D. A. Carter, J. M. Warnock, and B. B. Balsely, 1988: Temperature profiling using a UHF wind profiler and an acoustic source. Preprints, *Symp. on Lower Tropospheric Profiling: Needs and Technologies,* Boulder, CO, Amer. Meteor. Soc. 121–122.

Hallock, J. N., 1991: Aircraft wake vortices: An assessment of the current situation. U.S. Dept. of Transportation Rep. DOT-FAA-RD-90-29, 59 pp. [Available from National Technical Information Service, Sills Bldg., 5285 Port Royal Rd., Springfield, VA 22161.]

——, and W. R. Aberle, 1977: Aircraft wake vortices: A state-of-the-art review of the U.S. R&D Program. Federal Aviation Administration Rep. FAA-RD-77-23, 326 pp. [Available from National Technical Information Service, Sills Bldg., 5285 Port Royal Rd., Springfield, VA 22161.]

Hinton, D. A., 1996: An Aircraft Vortex Spacing System (AVOSS) for dynamical wake vortex spacing criteria. *AGARD Conf. Proc. 584, The Characteristics and Modification of Wakes from Lifting Vehicles in Fluids, Fluid Dynamics Panel Symp.,* Trondheim, Norway, AGARD, 1–12.

Marshall, J. M., 1970: A radio-acoustic sounding system for the remote measurement of atmospheric parameters. Radioscience Laboratory Rep. SU-SEL-70-050. [Available from Stanford University Engineering Library, Terman Engineering Center, 2nd Floor, Stanford, CA 94305-4029.]

——, A. M. Peterson, and A. A. Barnes Jr., 1972: Combined radar–acoustic sounding system. *Appl. Opt.,* **11,** 108–112.

May, P. T., R. G. Strauch, K. P. Moran, and W. D. Neff, 1989: High resolution weather observations with combined RASS and wind profilers. *Proc. 24th Conf. on Radar Meteorology,* Tallahassee, FL, Amer. Meteor. Soc., 746–749.

North, E. M., A. M. Peterson, and H. D. Pang, 1973: RASS, a remote sensing system for measuring low-level temperature profiles. *Bull. Amer. Meteor. Soc.,* **54,** 912–919.

Rubin, W. L., 1993: Glide slope surveillance sensor. U.S. Patent No. 5,208,600.

——, D. C. Burnham, E. A. Spitzer, and R. P. Rudis, 1999: A robust low cost airport wake vortex sensor. Preprints, *38th Aerospace Sciences Meeting,* Reno, NV, AIAA.

Spitzer, E. A., J. N. Hallock, and W. D. Wood, 1977: Status of the vortex advisory system. *Proc. Aircraft Wake Vortices Conf.,* Cambridge, MA, Federal Aviation Administration, 326–334.

Strauch, R. G., K. P. Moran, P. T. May, A. J. Bedard Jr., and W. L. Ecklund, 1989: RASS temperature soundings with wind profiler radars. Preprints, *24th Conf. on Radar Meteorology*, Tallahassee, FL, Amer. Meteor. Soc., 741–745.